



ASME Accepted Manuscript Repository

Institutional Repository Cover Sheet

First

Last

ASME Paper Title: Validation Studies of Linear Oscillating Compressor Cascade and Use of Influence

Coefficient Method

Authors: H. M. Phan and L. He

ASME Journal Title: Journal of Turbomachinery

Volume/Issue 142/5 Date of Publication (VOR* Online) 9/4/2020

ASME Digital Collection URL: <https://asmedigitalcollection.asme.org/turbomachinery/article/142/5/051005/1071624/Validation-Studies-of-Linear-Oscillating>

DOI: <https://doi.org/10.1115/1.4045657>

*VOR (version of record)

Validation Studies of Linear Oscillating Compressor Cascade and Use of Influence Coefficient Method

H. M. Phan¹

Department of Engineering Science, University of Oxford, Oxford, United Kingdom
(hien.phan@eng.ox.ac.uk)

L. He

Department of Engineering Science, University of Oxford, Oxford, United Kingdom

ABSTRACT

Advanced predictions of blade flutter have been continually pursued. It is noted however that validation cases of unsteady CFD methods against experimental cases with detailed 3D unsteady pressures are still rather lacking. The main objectives of the present work are two-folds. Firstly, validate and understand the characteristics of blade tip clearance, as well as a bubble-type flow separation for an unsteady CFD solver against a 3D oscillating cascade experiment. And secondly, examine the applicability of the Influence Coefficient Method (ICM) as widely used in an oscillating linear cascade setup.

In the first part, the capability of a widely used commercial solver (CFX) for unsteady flows induced by a 3D oscillating compressor cascade is examined. The present computations have shown consistently a destabilizing effect of increasing blade tip clearance, in agreement with the experiment. More remarkably, the computational analyses reveal a distinctive interplay between the inlet endwall boundary layer and the tip clearance in relation to the aerodynamic damping. Different inlet endwall boundary layer thicknesses are shown to lead to qualitatively different aeroelastic stability characteristics in relation to tip clearance. The aero-damping variation with the tip-clearance under the influence of the inlet endwall boundary layer seems

¹ Corresponding author

to correlate closely to a balancing act between the passage vortex and the tip-leakage vortex. The tip clearance aeroelastic behaviour seems also in line with a simple quasi-steady analysis. On the other hand, the mid-chord laminar bubble separation on suction surface, though with a clear signature in the local aero-damping, has negligible effects on the overall stability.

The second part aims to examine computationally the applicability of the influence coefficient method in a linear cascade setup. The comparison between the cascade based ICM data and a baseline ‘tuned cascade’ shows that the differences in the sensitivity to the far-field treatment can be significant, depending on interblade phase angles. On the other hand, non-linearity effects closely relevant to the basic linear assumption of the ICM are shown to only have a small influence. The present results suggest that extra caution should be exercised when comparing a CFD-based tuned cascade model with a finite cascade-based ICM model, at conditions close to acoustic resonance. The resultant discrepancies may well arise from the inherently different far-field sensitivities between the two models, rather than those typical numerical and physical modelling aspects of interest (e.g. meshing, spatial and temporal discretization errors as well as turbulence modelling).

1 INTRODUCTION

Among the blade aeroelasticity problems, flutter is a common phenomenon that affects blade rows with a high aspect ratio such as frontal stages of compressors and rear stages of turbines. Previous researchers have shown that the mechanisms of flutter are complex and many factors are involved. The fundamental oscillating bladerow model is the one in a traveling wave ‘tuned cascade’ mode characterized by all blades in the row oscillating at the same frequency and with a constant phase difference between adjacent blades [1]. Correspondingly, two basic variables are closely relevant to blade aeroelastic stability, namely the reduced frequency and interblade phase angle.

Various experimental results of both compressor and turbine cascades at various operating conditions are available in the public domain. Notably, Bölcs and Fransson [2] established the Standard Configurations for the benchmark tests and computational method validations. However, the published detailed measurements are usually limited at mid-span 2D sections [3-5]. Given the 3D nature of turbomachine blades, the understanding of fully three-dimensional features and their impact on the aeroelastic stability is important. Widely developed CFD solvers for blade flutter prediction also need 3D experimental cases for validation. Bell and He [6] showed the influence of varying spanwise bending amplitude for the first time, although the cascade comprised only one blade. Subsequently, Yang and He [7] carried out an experiment to measure the spanwise damping distribution on the compressor cascade at different tip clearances. A similar 3D experiment was conducted by Huang et al. [8] but on a linear turbine cascade. A further research on the same oscillating turbine cascade was carried out experimentally and computationally with the part-span shrouds [9]. A more recent study involves a compressor cascade with suction side squealer [10]. An annular sector cascade is sometimes used instead of the conventional linear cascade [11]. Some recent efforts are aimed to experimentally study the flutter mechanism in a transonic linear cascade [12,13].

Blade tip leakage is an important three-dimensional flow feature that has attracted much attention from various researchers in the past. It is widely accepted that tip clearance is detrimental to compressor aerodynamic losses, stall inception and margin, e.g. [14,15]. Fewer researchers have studied the behaviour and impact of tip clearance

on the compressor flutter stability, but there is however still lack of consistent findings. Yang and He [7] showed a destabilizing effect when the tip clearance was increased in their low speed linear cascade experimental case subject to oscillation in a bending mode. Besem and Kielb [16] investigated computationally the effects of tip clearance for rotor blades oscillating in a torsion mode, but found a non-monotonic variation of aero-damping with tip clearance. The damping initially increased with the tip gap size until it reached a maximum and it then decreased with the further tip gap increases. And overall, the tip gap seemed to have a stabilizing effect compared to the zero tip-gap case [16]. On the other hand, Fu et al. [17] studied numerically blade oscillation in a bending mode for transonic rotor which was observed to subject to flutter during the rig test. They showed that the aero-damping decreased with increasing tip gap until it reached a minimum, then an opposite damping variation with tip gap was observed. This finding is in contrast to that of Besem and Kielb [16]. Overall, the previous studies of tip-leakage effects on the compressor blade aeroelastic stability still remain inconclusive.

The present work is prompted by the recognition of the lack of detailed 3D experimental data for oscillating blades for understanding the impact of tip clearance behaviour on aerodynamic damping and for validating 3D unsteady CFD solvers. In particular, commercial CFD solvers, which have been extensively validated and applied to turbomachinery flow analyses, have recently began to be utilized in blade aeroelasticity analyses. This underpins the often-overlooked need for validations of these codes in turbomachinery aeroelastic applications. Thus, the first primary objective of the present

work is to validate a commercial solver (CFX) in predicting unsteady aerodynamics induced by a three-dimensional oscillating compressor cascade.

Another issue of interest in blade aeroelastic modelling is related to the Influence Coefficient Method (ICM). Proposed by Hanamura et al. [18], this is the most common method in getting equivalent tuned cascade data from experimental linear cascades and annular sector rigs with only the middle blade oscillating, e.g. [4,5,7,8,9,10,11,13]. The validity of the ICM has been commonly judged mainly in terms of linearity of the unsteady flow, thus the applicability of superposition. However many researchers in the field have been somewhat concerned and puzzled by the inter-blade phase angle dependent discrepancies between tuned cascade predictions and linear cascade derived ICM data, particularly in certain ranges of inter-blade phase angles (some confusions in relation to this issue are expressed in the presentations and discussions in a few blade aeroelasticity sessions in some recent ASME/IGTI conferences). Given the experimental data to be used in the present work is also from an ICM based linear cascade, it seems appropriate to also examine closely its validity and applicability. A basic question is, *what should one expect when comparing the aero-damping results with respect to inter-blade phase angles between a tuned cascade model and an ICM-model based linear cascade?* The second part of the paper is a computational study carried out with the standard setup in a commercial code as one would use for a typical blade aeroelastic analysis. The comparative case studies serve to highlight the important difference between the two models and the conditions at which extra caution should be taken, additionally to the common issue of linearity.

2 TEST CASE

2.1 Description

The compressor blade profile used in this study is the controlled-diffusion blading proposed by Elazar et al. [19], which has been studied extensively for its steady performance in modern blade profile designs. The blading was utilized in an oscillating cascade test but operated at a reduced Reynolds number. At the original design Reynolds number, $Re = 7 \times 10^5$, there is no bubble separation identifiable. The same blading was adopted in an oscillating cascade experiment at a lower Reynolds number of $Re = 1.95 \times 10^5$ (Yang and He [7]). At this lower Re , a laminar bubble separation forms around mid-chord on the suction surface. Recently, He and Yi [20] employed a high fidelity two-scale methodology for URANS/LES to study this blade profile, also predicting the separation bubble.

Although the cascade was studied at a low-speed condition, it involves with various important features in gas turbine aerodynamic blading design, including laminar bubble separation and tip clearance. A laminar bubble type separation with subsequent transition to turbulent flow is relevant to turbomachinery design applications for both turbines and compressors in general. For compressors in particular, the laminar separation-transition on a blade suction surface is also closely relevant to aerodynamic performances, as extensively studied in the past, e.g. by Dong and Cumpsty [21], Halstead et al. [22], Cumpsty et al. [23]. Thus, it is of interest to assess the aeroelastic impact and predictability of a mid-chord laminar bubble separation on a compressor cascade, although there has been rarely any published work in this aspect so far.

The detailed measurement of unsteady pressures on different spanwise sections over the blade surfaces, especially in the near tip region makes this case suitable for validating modelling techniques and methods, and for exploring and understanding flow physics.

Table 1 shows a comparison between experimental and simulated operating conditions. Reynolds number Re and reduced frequency k are matched to a less than 5% discrepancy from the experimental conditions.

2.2 Data Reduction

A tuned cascade is characterized by all blades oscillating at the same frequency, the same amplitude and a constant phase angle difference between adjacent blades (IBPA). Effectively all the blades in the bladerow are oscillated in a circumferential travelling wave pattern, thus a tuned cascade model is also known as in a travelling wave mode (TWM). The unsteady pressures along a blade surface are collected during a period of vibration. The unsteady pressures are decomposed into temporal Fourier harmonic components:

$$p(t) = a_0 + \sum_n [a_n \cos(n\omega t) + b_n \sin(n\omega t)] = a_0 + \sum_n A p_n \sin(n\omega t + \phi_n) \quad (1)$$

For a blade oscillated in the sinusoidal motion, only the 1st harmonic pressure does aero-work (Work Sum) on the blade.

$$W_{aero} = \pi A m_l A p_1 \sin(\theta_1) \quad (2)$$

The local aerodynamic damping is normalized by the blade tip vibration amplitude and the isentropic exit dynamic head.

$$\xi_l = \frac{-W_{aero}}{(P_{01} - P_2) A m_{tip}^2} = \frac{-\pi A m_l |C p_1| \sin(\phi_1)}{A m_{tip}} \quad (3)$$

The overall damping is calculated by integrating the local damping along the blade chord and span:

$$\xi_c = \frac{1}{c} \int_0^c \frac{-\pi A m_l |C_{p1}| \sin(\phi_1)}{A m_{tip}} ds \quad (4)$$

$$\xi = \frac{1}{h} \int_0^h \xi_c dz \quad (5)$$

The influence coefficient method (ICM) is employed in both the experimental and the present computational study to obtain the overall damping for different interblade phase angles (IBPA). As such the whole range of the damping-IBPA variation for a given frequency can be obtained, as commonly required. The key feature, particularly important for experimental setups, is only one blade (blade '0' in the middle, Fig.1) in the cascade needs to be oscillated. Under the assumption of linear superposition, the unsteady aerodynamic influences on a reference blade from all oscillating blades in a tuned cascade (TWM) is equivalent to the sum of unsteady aerodynamic influences of one blade oscillating on itself and on all other non-oscillating blades in the cascade. Therefore, the first harmonic pressure coefficient of the reference blade (central blade) in TWM can be calculated as a sum of first harmonic pressure coefficients from the oscillating blade itself and its neighbouring stationary blades:

$$C_{p1} = \sum_{m=-3}^{+3} C_{p1}(m) e^{-im\sigma} \quad (6)$$

The IBPA σ is defined as positive for a forward travelling wave mode, where blade +1 leads blade 0 (see Fig.1).

3 NUMERICAL METHOD

3.1 Computational Domain Configuration

The computational study is conducted in the time domain. The central blade is oscillated in the bending mode, whereas other blades are kept stationary as in the influence coefficient method. The ICM computational model includes a five-blade configuration with a direct periodicity.

Preliminary study has been conducted on a 2D mid-span section to assess the number of required passages. The number of blades passages required for getting an adequate result for tuned cascade is indicated by the decaying rate of the unsteady disturbances always from the middle blade. This effectively corresponds to how fast the summation of influence coefficients (Eq. 6) would converge, thus it may be called the ICM 'convergence' characteristics. Fig. 2 shows the corresponding aerodynamic damping components contributed from each blade in the cascade with the middle oscillating blade B0.

The convergence characteristics shown in Fig. 2 suggest that only the oscillating blade (B0) and two immediate blades at vicinity to its suction and pressure surfaces (B+1 and B-1) are significant in the aero-damping calculation. Hence, the ICM computational model with five blades is deemed reasonable for the present case.

3.2 Boundary Conditions

The commercial solver CFX 18.2 is used for the simulations. The inlet boundary conditions include total pressure, total temperature, and flow angle. The static atmospheric pressure is used at the outlet. The blades, hub, and casing surfaces are modelled as an adiabatic no-slip wall. For unsteady simulations, the central reference blade is oscillated in a prescribed blade motion, with a linear amplitude variation from the tip to hub. A translational periodicity is applied at two outermost interfaces to

represent an infinite linear cascade. For unsteady simulations of tip clearance cases, the volume mesh of the tip region above the central blade is periodically deformed together with the central blade mesh to avoid mesh folding.

3.4 Computational Mesh

Meshing is carried out in ICEM to generate a high-quality unstructured hexahedral volume mesh. HOH topology is used to create H mesh in the inlet and outlet blocks. The main domain containing the blades are modelled with O grid around the blade surfaces to resolve the boundary layers. Fig. 3 shows a computational multi-block mesh with local refinement around the leading edge.

4 STEADY FLOW RESULTS

4.1 Sensitivity to Turbulence and Transition Modelling

The laminar bubble separation is captured on the suction surface in the experiment. In the computational study, the turbulence sensitivity shows that only the two-equation γ - θ transition correlation coupled with the SST model [24] is able to predict the separation bubble numerically. Fig. 4 presents the axial Mach number contours predicted by both the transitional and the fully turbulent models. The laminar separation bubble is clearly identified by the zone of negative axial Mach number, which indicates a flow reversal region.

Fig. 5 shows the improved predictability of the transitional model from 30% to 50% chord. This computed bubble separation agrees with the experimental results, whereas the boundary layer remains attached if the fully turbulent model is used.

4.2 Effect of Inlet Endwall Boundary Layer

One of the notable feature of this cascade as experimentally observed is the unloading effect near the endwall. If the uniform total pressure is applied at the inlet (i.e. the endwall boundary would only start to grow from the inlet plane), no significant unloading near the endwall can be observed in the computational results. Fig. 6a presents the steady pressure distributions at 50% and 95% spans for the simulation with the uniform inlet boundary condition. There is hardly any unloading in the tip region in the computed results, clearly in disagreement with the experimental data.

The key parameter, as it turns out, is the thickness of inlet endwall boundary layer. Using the inlet endwall boundary layer thickness as reported by Williams et al. [25], a much improved prediction is obtained (Fig. 6b). The significant unloading effect can now be well captured at 95% span, agreeing with the experiment.

4.3 Effect of Tip Clearance

In the experiment, the tip clearance is changed by relocating the blade relative to the perspex endwall in the spanwise direction, while the pressure tapping locations and the cascade casing are fixed. Hence, the percentage span is defined as the location of the pressure tapping relative to the original blade span. The same definition is used in the simulations for tip clearance cases for consistency.

Fig. 7 presents the steady pressure distributions at 95% span for different tip gaps. Again the results with the profiled inlet (Fig. 7b) and those with the uniform inlet (Fig. 7a) are contrasted. There are three regions of surface pressure variations with the tip clearance, to be noted firstly from the experimental data.

- i) The frontal region from the leading edge to 25% chord. This is the part where the pressures on the suction surface increases (off-loading) when the tip gap increases;
- ii) The region between 25% and 50% chord. Here the pressure variation is opposite to that of the frontal part. The pressure decreases (up-loading) when the tip gap increases;
- iii) The rear part from 50% chord to the trailing edge. In this region, the pressures vary non-monotonically with the tip gap. They first increase (off-loading) when the tip gap increases from 0% to 1%. Then when the tip gap further increases from 1% to 2%, the pressures in this rear part decrease (up-loading).

More relevantly to the present interest, we note that the steady pressure variations with the tip gap are well predicted when the inlet end wall boundary profile is introduced (Fig. 7b). The correct trends for all three regions are well captured in agreement with the experiment, though the detailed distributions in the rear region, particular at the largest tip gap (2%) can only be regarded as fair, which should be reasonably expected given the complexity of the corresponding leakage flow.

On the contrary, the pressures predicted with the uniform inlet are in serious errors in the overall loading for all tip gaps (Fig. 7a). Furthermore, for the rear part of the suction surface, the pressure distributions even have a different trend of variation with the tip gap, compared to the experimental one.

5 UNSTEADY FLOW RESULTS

5.1 Aeroelastic Damping of Tuned Cascade

Fig. 8 shows the overall damping at reduced frequency $k = 0.2$ and 0.4 . The CFD results are in good agreement with the experiment. The least stable IBPA lies in the

forward travelling wave mode, at about 20° to 30° of IBPAs. Both computational and experimental aero-damping curves seem to follow the trend that as the reduced frequency k decreases, the damping curve moves downward (towards the instability zone) and rightward (towards the forward travelling wave mode zone). This is also in line with the industry experience in the way that the reduced frequency k can be increased by increasing the blade chord and/or the blade thickness to improve the aeroelastic stability.

5.2 Aeroelastic Effect of Separation Bubble

In the previous part, the laminar separation bubble on the suction surface in the middle span region has been shown to affect the local steady pressure distribution. On the aeroelastic stability, experimental local damping distributions on the suction surface reveals marked local variations around the laminar separation - attachment point. This transitional behaviour is in good agreement with the configuration adopting the transitional turbulence model, whereas the fully turbulent model completely misses this behaviour.

Fig. 9 shows the overall damping at the mid-span section. Despite the marked difference in the local damping on the suction surface between the transitional and fully turbulent models, the overall damping values over the entire blade chord are not significantly affected, particularly in the IBPA regions with a minimum damping. Therefore, for the present case the suction surface laminar bubble separation does seem to be insignificant as far as the overall damping is concerned.

The present observation is also in line with the previous finding for an oscillating turbine cascade configuration, for which the bubble-type flow separation on the suction surface was shown to have relatively a small influence on the overall aerodynamic damping, both experimentally and computationally [4,26].

5.3 Aeroelastic Effect of Tip Clearance

5.3.1 Overall Aero-Damping Variation with Tip Gap

Fig. 10 shows the effects of tip clearance on the overall damping. It can be seen that the least stable damping decreases as the tip gap increases. The least stable IBPA remains almost the same, to be about 20-30 degrees. The predicted destabilizing trend of increasing tip clearance is captured qualitatively across the entire range of IBPA, compared to the experiment. When the tip gap increases from 0% to 2%, the calculated minimum damping is decreased by about 27%. From the experiment, the minimum damping was also reduced by about 27% compared to that at the nominal zero tip-gap condition. This is a quite considerable damping reduction considering how much the damping is decreased when the reduced frequency k is halved from 0.4 to 0.2 as shown in Fig. 8, although the very quantitative agreement with the experiment should not be taken to reflect a typical level of accuracy to be expected.

A close inspection of the minimum damping values at the least stable IBPA is taken as shown in Fig. 11. It can be seen that the computations with the uniform inlet condition predict a rather insignificant reduction in the minimum damping when the tip gap is changed from 0 to 2% span. However a marked reduction of the damping with the tip clearance is observed in the CFD with the inlet endwall boundary layer profile, predicting

about a damping drop of about 27% with the increase of the tip clearance, in good agreement with the experiment.

5.3.2 Local Aero-Damping and Quasi-Steady Analysis

To help understand the underlying flow physics that drives the aero-damping characteristics, we now examine the local damping distributions on blade surfaces. The main attention is directed to the blade suction surface where major contributing factors are at play when the tip clearance is changed. Fig. 12 shows the local damping contours on the suction surface at two tip clearances. Two distinctive regions are noted.

- a) The bulk frontal part (marked as '**A**' in Fig. 12) from the leading edge to about 30% chord, and for most of the span from the tip down to nearly 20% span. This is a region with a strong stabilizing effect regardless of the tip gap.
- b) The rear part from 30% chord to the trailing edge in the tip region (marked as '**B**'). This is the part where the destabilizing effect of the tip clearance and its increased strength at a larger tip gap are clearly identifiable.

The bulk frontal part "A" is deemed to be largely independent of the tip gap as the affected stabilizing area stretches well into the mid-span and beyond. A following simple quasi-steady analysis may be used to explain the behaviour.

The bending displacement in the y-direction normal to the chord and the corresponding unsteady aerodynamic force on the blade in this direction f can be expressed as:

$$y = A_y \sin(\omega t) \quad (7)$$

$$f = A_f \sin(\omega t + \varphi_f) \quad (8)$$

At the mean position with $\omega t = 0^0$ (shown in Fig. 13a), the vibratory velocity V_y in the y-direction is at its maximum. Given the absolute inflow velocity V_1 , the velocity diagram would give a relative velocity (W_1) corresponding to a negative incidence. Thus, the leading edge portion of the blade is off-loaded, leading to a higher local pressure near the L.E. on the suction surface. In terms of the blade force in y-direction, this local high pressure peak on the suction surface should correspond to a negative contribution to the blade force in the y-direction. Thus the corresponding unsteady force has a 90^0 phase lag (i.e. $\varphi_f = -90^0$). This part then has a positive damping contribution. Hence we can see that the bulk frontal part is predominantly subject to a stabilizing incidence effect localized around the leading edge.

For the rear part near tip (marked as 'B' in Fig. 12), the negative damping has an apparent signature of the tip leakage. Once again, a quasi-steady analysis may be used. Basically, the over-tip leakage ('OTL') flow is driven by the pressure difference between pressure and suction surfaces. The leakage flow is also resisted by the shear stresses from the tip and casing surfaces. For the oscillating blade, we focus on the wall friction shear stresses on the over-tip surface (' τ_w ' in Fig. 13b). The tip vibratory motion can enhance or suppress the leakage flow, depending on the velocity of the movement. At the mean position ($\omega t = 0^0$), the tip velocity (V_y) is at its maximum in the direction from the pressure surface to the suction one (Fig. 13b). An increase in the surface velocity should lead to a decrease in the velocity gradient (thus a drop in shear stress ' τ_w '). Correspondingly at this moment with a minimum friction on the tip surface, the tip leakage flow should be roughly at its highest. Recall the steady pressure distributions near

the tip at different tip gaps discussed earlier. For the rear portion of the suction surface, an increase in the tip leakage flow would correspond to a decrease in local pressures (up-loading) when the tip gap is increased from 1% to 2% (Fig. 7b). Thus at $\omega t = 0^0$, we have the minimum pressures on the rear suction surface, i.e. the local pressures lag the blade movement by 90° . The corresponding local suction force contribution to the overall unsteady force would have a 90° phase lead (i.e. $\varphi_f = 90^\circ$ in Eq.8). Therefore, we should expect a local negative damping contribution in the rear tip region 'B' due to the tip clearance, as observed.

5.3.3 Balancing Tip Leakage Vortex with Passage Vortex

Finally some further understanding on the marked impact of inlet endwall boundary layer profile can be gained by considering the interaction between two main vortices (passage vortex and tip leakage vortex) in a blade passage. Shown in Fig. 14 are velocity vectors and vorticity contours on several axial cut planes for the case with a uniform inlet. The corresponding results for the case with the inlet boundary layer profile are shown in Fig. 15.

The flow with zero tip clearance (Fig. 14a and Fig. 15a) should serve as a baseline before the tip clearance effect is examined. A strong passage vortex (PV) is seen under the condition of the inlet endwall boundary layer (Fig. 15a). On the other hand for the uniform inlet case (Fig. 14a), the passage vortex is rather weak and not easily identifiable. This is in line with previous research findings that a thicker inlet endwall boundary layer would more effectively promote the cross-passage flow from the pressure surface to the suction surface [27]. This strong secondary flow is mainly responsible for the off-loading

near the tip as observed in the measured steady pressures as shown in Fig. 7b (noting that the off-loading exists for the zero tip gap).

When the tip clearance is introduced, the base flow setup by the passage-vortex is noticeably changed near the suction surface side. The secondary flows near the pressure side remains similar to the cases at the zero tip gap. Now the tip leakage vortex (TLV) seems to be more compact with the uniform inlet flow (Fig. 14b) than that with the inlet endwall boundary layer (Fig. 15b).

In the case of the uniform inlet, there is far less off-loading near the endwall when the tip gap is increased, as seen in the pressure distributions (Fig. 7a). This might be largely attributed to that the base flow responsible for the near tip off-loading is chiefly set up by the passage vortex associated with the secondary flow. And in this case, the two qualitatively different base flows are set up by the two different inflow conditions.

The different base flows may also explain the seemingly different sizes of the tip leakage vortices (TLV) between the two cases. The TLV for the uniform inlet is not strongly mixing out with the primary stream which has much higher velocity/inertia, and appears to be more confined (Fig. 14b). On the other hand, the TLV seems to interact more strongly with the passage vortex as the base flow is now subject to much stronger cross-passage secondary flow (a weaker primary flow). As a result, the TLV in this case appears bigger (Fig. 15b).

Overall, the interaction and balance between the TLV and the PV are shown to have important effects on the blade loading near the endwall. The close link of the relative strengths of the two primary vortices to the inlet endwall boundary layer thickness can

now be clearly seen. Thus one should not be surprised that different inlet endwall boundary layer thickness can lead to qualitatively differences in blade loading and subsequently aero-damping characteristics in the tip region.

6 ON VALIDITY OF INFLUENCE COEFFICIENT METHOD

6.1 Specific Issues of Interest

In the first part of this study, the direct periodicity was adopted in the ICM model to investigate the tip clearance effects in a compressor cascade. Due to the periodic interfaces in the computational model, the flow field is spatially periodic. However, in a practical experimental setup, the cascade configuration has a finite number of blades subject to upper and lower sidewalls as illustrated in Fig. 1 whether the cascade is of linear or sector annular type. With the presence of tunnel sidewalls, the spatial periodicity is more difficult to achieve, particularly for the outermost blades. In an experiment, a better flow field periodicity and uniformity can be managed by a combination of treatments such as wall suction and tailboard angles alignment. CFD modelling of these additional effects is complicated and not covered in this current work. Hence, the validity of the influence coefficient method in a conventional setup representing a realistic experimental configuration is what we are concerned about. In this part, the tunnel sidewalls are modelled as the inviscid-slip wall from the inlet to the leading edge station to avoid the ambiguity of blockage effects due to the build-up of boundary layers in this region. At the lower and upper boundaries of the tunnel sidewalls, the no-slip wall condition is applied.

There are two basic assumptions of the ICM for a linear (or an annular sector) cascade bounded by two sidewalls:

- 1) The cascade contains a sufficient number of blades so that the unsteady pressures on the furthest blades from the middle oscillating blade will be of a negligible amplitude. This is required for the convergence of the influence coefficients summation based on the finite number of blades in the cascade (Eq. 6);
- 2) A linear behaviour of the unsteady pressures induced by the middle oscillating blade, thus the validity of superposition.

Regarding the first aspect, the decay of unsteady pressure responses of blades with its distance from the oscillating blade is required. The convergence behaviour of the ICM model has been discussed earlier in relation to the results as shown in Fig. 2.

The second aspect is the linearity assumption. A test of the linearity is carried out by comparing the unsteady pressure responses computed at two bending oscillation amplitudes, 6%C and 3%C and that measured from the experiment at mid-span, as shown in Fig. 16. The first harmonic pressure amplitude distributions calculated using the ICM model from the two amplitudes are almost identical, except near the leading edge and the separation bubble region. Similar observation is also made from the experimental results. Hence, despite of a slight nonlinearity, its overall contribution to the aero-damping is deemed to be negligible for this case.

Having examined the validity of the two common assumptions, we now turn our attention to the sensitivity and implications of the far-field conditions, as the main focus of this study. It is worth noting that the ICM-based data from a linear or annular sector cascade are commonly used to generate tuned cascade data for an entire range of IBPAs (e.g. Fig. 10). As such it seems to be taken for granted or implied that a standard tuned

cascade model where all blades are oscillating in a travelling wave mode (TWM) should be directly comparable to an ICM-generated tuned cascade results at any IBPA. A question to be asked is that in addition to the basic assumptions as examined above, is there any other factor at play in terms of the validity and applicability of the influence coefficient method in a linear or annular sector cascade set up?

It is observed that the present ICM-based damping variations with IBPA all seem quite smooth and sinusoidal. However, LINSUB [28], a 2D semi-analytical code for unsteady flows past a tuned flat plate cascade, shows clearly unsmooth aero-damping curves, as seen in Fig. 17. These spikes are due to the dynamic behaviour of the inlet and outlet ducts rather than flow physics inside the bladerow. The spikes in the unsteady responses happen around a resonance condition of an annular duct acoustic mode corresponding to a certain circumferential wave length and travelling speed (thus frequency and IBPA). Given these very contrasting observations we would like to further examine the sensitivity of the two models (TWM vs ICM) to far-field inlet and outlet treatments.

The annular duct acoustic resonance conditions can be estimated based on Eq. 9 [28]. The phase angles that cause acoustic resonance satisfy the conditions that the waves carry energy in a purely circumferential direction, so no energy is lost by radiation in an axial direction. For a subsonic flow, Eq. 9 gives two discrete angles, a negative σ_R^- and a positive σ_R^+ resonance IBPA phase angle. The flow is cut-on i.e. the acoustic waves propagate when the IBPA is in the range, $\sigma_R^- < IBPA < \sigma_R^+$. M , M_x , and M_y are the total, axial, and circumferential Mach numbers, respectively. k is the reduced frequency and S/C is the pitch-to-chord ratio.

$$\sigma_R = (M_y \pm \sqrt{1 - M_x^2}) Mk(S/C)/(1 - M^2) \quad (9)$$

6.2 Test Configurations and Conditions

In order to examine the sensitivity of aeroelastic response of the cascade to the far-field treatment, the domain duct lengths are varied to alter the acoustic behaviour of the system. The inlet and outlet duct lengths are increased to about 2C and 5C, respectively. The extended long duct domain is covered with a coarse mesh stretched in the axial direction with an extra numerical damping effect on the far field.

The Fourier Transformation method implemented in CFX in a double-passage domain with the phase-shifted periodicity is used for TWM simulations. In this method, the flow history on the phase-shifted periodic boundaries are stored and reconstructed using Fourier series based on the work of He [29].

6.3 Low-speed Cases

Fig. 18 presents the overall damping of configurations with different duct lengths predicted by both the influence coefficient method and the tuned cascade model. At this low Mach number, the acoustic resonance is estimated to occur between $\sigma_R^- = -1.4^0$ and $\sigma_R^+ = +1.6^0$ based on Eq. 9. The computations of both ICM and TWM seem not to be able to capture the acoustic resonance and the overall damping curve is largely smooth and sinusoidal.

When the duct lengths are extended, the minimum damping changes by +36% for the ICM model and -31% for the TWM model. Importantly, the ICM and TWM models respond in an opposite way when the duct length is extended. The ICM model is shown to be more

stabilizing, whereas the TWM model is shown to be more destabilizing as the duct length is extended.

Fig. 19 presents the first harmonic unsteady pressure amplitudes for both the ICM and the TWM models with different duct length configurations at the forward travelling wave mode IBPA 30° and 180° , respectively.

At IBPA 30° (Fig. 19a), the far-field seems to be a cut-off but with a slow decaying rate of the pressure amplitude. There are some notable features for this case. Firstly the difference between different models are relative small for the short duct. But there are much larger differences between the two models for the long duct domain case. Interestingly, the ICM results for the long duct are rather similar to those of the short duct. On the other hand, the substantially different far-field acoustic behaviour of the tuned cascade model leads to a significant mismatch between the overall damping predicted by the ICM-generated and the TWM-based tuned cascade model (Fig. 19a). Thus the tuned cascade model (TWM) is shown to be much more sensitive to the far-field treatment, at this IBPA condition.

In contrast, the case at IBPA 180° (Fig. 19b) represents a well cut-off scenario with a very fast decaying rate. In this case further away from the acoustic resonance condition, the first harmonic unsteady pressure amplitudes in all configurations decay quickly to zero when approaching inlet and outlet far-field. As a result, the overall damping predicted by all configurations at IBPA 180° are almost identical.

A key observation from the above comparisons is the strong IBPA dependence of the sensitivity. It is worth underlining that the corresponding computations for the two IBPAs

are carried out with completely consistent mesh resolution, numerics, boundary conditions and turbulence modelling. This serves as a useful example to highlight that extra care should be taken when comparing results between a tuned cascade (TWM) model and a linear cascade based ICM model, especially at conditions close to an acoustic resonance.

6.4 High-speed Cases

The experimental rig is in a low-speed regime. Although we have had some useful observations, it would be naturally of interest to ask what we should expect in its high speed counterpart with seemingly more nonlinear transonic flows.

To address this, the current cascade is further studied numerically in a high-speed regime by reducing the static pressure at outlet ($P_2/P_{01} \approx 0.82$). The maximum isentropic Mach number of the blade is about 1.0 - 1.1 on the suction surface as shown in Fig. 20.

At this practically transonic flow condition, the linearity assumption of the ICM model is examined by considering various bending oscillation amplitudes: 1%C, and 0.5%C. The unsteady pressure responses show a bump in the first harmonic unsteady pressure amplitude on the suction surface, at the location where the isentropic Mach number enters the transonic regime. Comparisons of the unsteady pressure coefficients of the central oscillating blade for the ICM method (Fig. 21) show that this transonic bump is sensitive to the bending amplitude, and hence an indication of nonlinearity. At the small bending amplitudes (<1%C), the flow is largely linear. As the bending amplitude increases, the non-linearity increases as can be seen from the unsteady pressure responses at a

bending amplitude 3%. For practical high speed flutter predictions, this large amplitude is deemed to be too big. An amplitude of 1% or less would be deemed to be more appropriate. Therefore, for a given small oscillation amplitude, we can say that the linearity assumption of the ICM model should still hold even when the flow field enters a transonic regime.

On the numerical convergence, the travelling wave mode simulations at a high speed tend to be more difficult to achieve convergence to a periodic state. Additional numerical damping has to be applied for the high speed cases to remove numerical noises from a solution. It is noted that when a strong numerical damping is applied, the acoustic response in the far-field can also be damped significantly, and the overall damping can become smooth and sinusoidal as seen in the influence coefficient method for the low speed case. A similar effect of the numerical damping has been observed when the numerical boundary conditions can be regularized near acoustic resonance, such that the singularity behaviour near the acoustic resonance can become smoother [30].

Fig. 22 presents the overall damping variation with IBPA for different configurations by both the ICM and TWM methods. At this high Mach number condition, the acoustic cut-on condition is estimated to occur between $\sigma_R^- = -8.5^\circ$ and $\sigma_R^+ = +34.8^\circ$ based on the theoretical prediction (Eq. 9). The damping results of the TWM models seem to be more different from each other as well as from those of the ICM, particularly in the cut-on region bounded by two acoustic resonance IBPAs, indicating a higher sensitivity.

Similar to the case of the low speed flow, the ICM and TWM models are shown to respond very differently when the duct length is extended. The minimum damping is

increased by +101% for the ICM model. But for the TWM model, the minimum damping is reduced substantially. In fact the TWM solution damping becomes negative when the large duct domain is used. It is worth noting that the IBPA range with the largest discrepancies correspond to the cut-on region bounded by the acoustic resonance conditions.

The results of the high-speed case reinforces the observation from the low-speed test case. The unsteady flow response is still largely linear. There is a strong IBPA dependency of the damping comparison between the two models of interest. The sensitive regions are around the cut-on IBPAs range with relatively low aero-damping.

6.5 Further Discussion

The present computational studies indicate that the linear assumption of the ICM model is largely adequate for a range of flow conditions of practical interest, even in a transonic flow. So the influence coefficient model per se seems to be largely valid, at least as shown for the present cases tested.

However, we do see considerable differences in the results between the influence coefficient model as in the practical linear cascade experimental setup and the tuned cascade model. The differences are clearly dependent on IBPA for a given frequency. The prevailing factor causing the differences seems to be attributed to the inherent different far-field behaviour, manifested by that a tuned oscillating cascade model can excite an acoustic resonance in an annulus duct. On the other hand, the presence of tunnel sidewalls in a linear or annular sector cascade experiment will clearly affect the circumferential travelling waves. The pressure waves would reflect off the tunnel

sidewalls and feedback to the main flow field. This would ultimately affect the behaviour and sensitivity of the corresponding influence coefficient model to far-field conditions compared to its tuned cascade model counterpart.

It is also meaningful to make a distinction between the validity of the ICM model itself, and the applicability of the ICM for practical purposes. The present observations suggest that care should be taken when comparing the results between the ICM based on a linear cascade or annular sector cascade experiment and a tuned cascade TWM model for validation purposes.

In many cases, ICM-based experimental data are intended to be used to validate the near-field physical and numerical modelling aspects for oscillating blade rows (e.g. mesh, turbulence modelling, temporal and spatial discretization, geometrical modelling, unsteady viscous flow physics etc). In this case, caution should be exercised when comparisons with a tuned cascade model are made, particularly at conditions when the near-field bladerow unsteady aerodynamics and the aero-damping are highly sensitive to the far field acoustic behaviour and treatment.

7 CONCLUSIONS

The present study consists of two parts. In the first part, the unsteady CFD solver for oscillating blades as implemented in CFX has been validated against the detailed 3D experimental data of an oscillating compressor cascade. This is one of only few validation studies against detailed 3D unsteady aerodynamic experimental data available in the public domain. The following observations can be made:

- 1) The tip clearance is shown to have a destabilizing effect on the aeroelastic stability for the present compressor cascade, in agreement with the experiment.
- 2) There is a distinctive interplay between the inlet endwall boundary layer and the tip clearance in relation to the aerodynamic damping. Qualitatively different aeroelastic characteristics of tip clearance are observed when subject to different inlet endwall boundary layers.
- 3) The laminar bubble separation on the suction surface has a clear signature in the local aerodynamic damping distribution. However, it yields an insignificant effect on the overall damping.

In the second part, the validity and applicability of the influence coefficient method (ICM) in a linear cascade setup are examined, leading to the following observations:

- 1) The unsteady flow response in this cascade is predominantly linear for both low speed and high speed transonic conditions. The present results support the validity of the ICM model per se.
- 2) The main difference between the ICM and the tuned cascade model arises from the inherently different far-field acoustic behaviour. This leads to distinctively different sensitivities of the two models to far-field conditions and treatments. Therefore, cautions should be exercised when using a linear cascade based ICM for validation purposes. We should not expect to reproduce the tuned cascade results over an entire inter-blade phase angle range from the ICM-based experimental data, particularly around the IBPA conditions when the far-field acoustic behaviour becomes strongly influential.

ACKNOWLEDGMENT

The support from the EPSRC CDT in Gas Turbine Aerodynamics is much appreciated. The work is partly sponsored by the Chair of Computational Aerothermal Engineering Bursary.

NOMENCLATURE

IBPA	interblade phase angle, degrees
ICM	Influence Coefficient Method
PS	pressure surface
PV	passage vortex
SS	suction surface
TLV	tip leakage vortex
TWM	Travelling Wave Mode
Am_l	local bending amplitude
Am_{tip}	tip bending amplitude
Ap_1	amplitude of the first harmonic pressure, Pa
C	blade chord, m
C_{ax}	blade axial chord, m
$ Cp_1 $	amplitude of the 1 st harmonic pressure coefficient; $ Cp_1 = Ap_1/(P_{01} - P_2)/Am_{tip}$
Cp	blade surface pressure coefficient; $C_p = (P - P_2)/(P_{01} - P_2)$
f	frequency, Hz
h	blade span, m
k	reduced frequency; $k = \omega C/V_{ref}$

P_{01}	mid-span inlet total pressure, Pa
P_2	outlet static pressure, Pa
S	blade pitch, m
V_{ref}	reference isentropic exit velocity, ms^{-1} ; $V_{ref} = \sqrt{2(P_{01} - P_2)/\rho}$
x	axial chordwise distance, m
z	spanwise location, m
β_1	inlet flow angle, relative to axial direction, degrees
ξ	overall aerodynamic damping coefficient
ξ_c	spanwise aerodynamic damping coefficient
ξ_l	local aerodynamic damping coefficient
σ	interblade phase angle, IBPA, degrees

REFERENCES

- [1] Lane, F., 1956, "System Mode Shapes in the Flutter of Compressor Blade Rows," *J. Aeronaut. Sci.*, **23**(1), pp. 54-66. DOI: 10.2514/8.3502
- [2] Bölcs, A., and Fransson, T. H., 1986, "Aeroelasticity in Turbomachines. Comparison of Theoretical and Experimental Cascade Results," Communication No.13 Lab de Thermique Appliquee, Ecole Polytechnique Federale de Lausanne (EPFL), Switzerland.
- [3] Buffum, D. H., and Fleeter, S., 1990, "Oscillating Cascade Aerodynamics by an Experimental Influence Coefficient Technique," *AIAA J. Propul. Power*, **6**(5), pp. 612-620. DOI: 10.2514/3.23262
- [4] He, L., 1998, "Unsteady Flow in Oscillating Turbine Cascade: Part 1 - Linear Cascade Experiment," *ASME J. Turbomach.*, **120**(2), pp. 262-268. DOI: 10.1115/1.2841401
- [5] Vogt, D. M., and Fransson, T. H., 2007, "Experimental Investigation of Mode Shape Sensitivity of an Oscillating Low-Pressure Turbine Cascade at Design and Off-Design Conditions," *ASME J. Eng. Gas Turbines Power*, **129**(2), pp. 530-541. DOI: 10.1115/1.2436567
- [6] Bell, D. L., and He, L., 2000, "Three-Dimensional Unsteady Flow for an Oscillating Turbine Blade and the Influence of Tip Leakage," *ASME J. Turbomach.*, **122**(1), pp. 93-101. DOI: 10.1115/1.555432
- [7] Yang, H., and He, L., 2004, "Experimental Study on Linear Compressor Cascade with Three-Dimensional Blade Oscillation," *AIAA J. Propul. Power*, **20**(1), pp. 108-188. DOI: 10.2514/1.1280
- [8] Huang, X., He, L., and Bell, D. L., 2008, "Effects of Tip Clearance on Aerodynamic Damping in a Linear Turbine Cascade," *AIAA J. Propul. Power*, **24**(1), pp. 26-33. DOI: 10.2514/1.25174
- [9] Huang, X., He, L., and Bell, D. L., 2009, "Experimental and Computational Study of Oscillating Turbine Cascade and Influence of Part-Span Shrouds," *ASME J. Fluids Eng.*, **131**(5), p.051102. DOI: 10.1115/1.3111254
- [10] Ma, H., Jin, C., and Wei, W., 2017, "Experimental Investigation of Effects of Suction Side Squealer Tip on The Aeroelastic Stability of a Linear Oscillating Compressor Cascade," *P. I. Mech. Eng. G - J. Aer.*, **231**(11), pp. 2120-2131. DOI: 10.1177/0954410016662057
- [11] Vogt, D. M., 2005, "Experimental Investigation of Three-Dimensional Mechanism in Low-Pressure Turbine Flutter," PhD Thesis, Royal Institute of Technology, Sweden.
- [12] Tian, S., Petrie-Repar, P., Glodic, N., and Sun, T., 2018, "CFD Aided Design of a Transonic Compressor Cascade Wind Tunnel," In 15th International Symposium on Unsteady Aerodynamics, Aeroacoustics and Aeroelasticity of Turbomachines ISUAAAT15, Oxford.
- [13] Watanabe, T., Azuma, T., Uzawa, S., Himeno, T., and Inoue, C., 2018, "Unsteady Pressure Measurement on Oscillating Blade in Transonic Flow Using Fast-Response Pressure-Sensitive Paint," *ASME J. Turbomach.*, **140**(6), p.061003. DOI: 10.1115/1.4039180
- [14] Storer, J. A., and Cumpsty, N. A., 1991, "Tip Leakage Flow in Axial Compressors," *ASME J. Turbomach.*, **113**(2), pp. 252-259. DOI: 10.1115/1.2929095

- [15] Camp, T. R., and Day, I. J., 1998, "A Study of Spike and Modal Stall Phenomena in a Low-Speed Axial Compressor," *ASME J. Turbomach.*, **120**(3), pp. 393-401. DOI: 10.1115/1.2841730
- [16] Besem, F. M., and Kielb, R. E., 2016, "Influence of the Tip Clearance on a Compressor Blade Aerodynamic Damping," *AIAA J. Propul. Power*, **33**(1), pp. 227-233. DOI: 10.2514/1.B36121
- [17] Fu, Z., Wang, Y., Jiang, X., and Wei, D., 2015, "Tip Clearance Effects on Aero-elastic Stability of Axial Compressor Blades," *ASME J. Eng. Gas Turbines Power*, **137**(1), p. 012501. DOI: 10.1115/1.4028019
- [18] Hanamura, Y., Tanaka, H., and Yamaguchi, K., 1980, "A Simplified Method to Measure Unsteady Forces Acting on The Vibrating Blades in Cascade," *Bulletin of JSME*, **23**(180), pp. 880-887. DOI: 10.1299/jsme1958.23.880
- [19] Elazar, Y., and Shreeve, R. P., 1990, "Viscous Flow in a Controlled Diffusion Compressor Cascade with Increasing Incidence," *ASME J. Turbomach.*, **112**(2), pp. 256-265. DOI: 10.1115/1.2927642
- [20] He, L., and Yi, J., 2017, "Two-Scale Methodology for URANS/Large Eddy Simulation Solutions of Unsteady Turbomachinery Flows," *ASME J. Turbomach.*, **139**(10), p.101012. DOI: 10.1115/1.4036765
- [21] Dong, Y., and Cumpsty, N. A., 1990, "Compressor Blade Boundary Layers: Part 2- Measurements With Incident Wakes," *ASME J. Turbomach.*, **112**(2), pp. 231-240. DOI: 10.1115/1.2927637
- [22] Halstead, D. E., Wisler, D. C., Okiishi, T. H., Walker, G. J., Hodson, H. P., and Shin, H. W., 1997, "Boundary Layer Development in Axial Compressors and Turbines: Part 2 of 4-Compressors," *ASME J. Turbomach.*, **119**(3), pp. 426-444. DOI: 10.1115/1.2841142
- [23] Cumpsty, N. A., Dong, Y. Y., and Li, Y. S., 1995, "Compressor Blade Boundary Layers in the Presence of Wakes," *ASME Paper No. 95-GT-443*. DOI: 10.1115/95-GT-443
- [24] Menter, F. R., Langtry, R., and Völker, S., 2006, "Transition Modelling for General Purpose CFD Codes," *Flow, Turbul. Combust.*, **77**(1-4), pp. 277-303. DOI: 10.1007/s10494-006-9047-1
- [25] Williams, R., Gregory-Smith, D., He, L., and Ingram, G., 2010, "Experiments and Computations on Large Tip Clearance Effects in a Linear Cascade," *ASME J. Turbomach.*, **132**(2), pp. 021018. DOI: 10.1115/1.3104611
- [26] He, L., 1998, "Unsteady Flow in Oscillating Turbine Cascade: Part 2 – Computational Study," *ASME J. Turbomach.*, **120**(2), pp. 269-275. DOI: 10.1115/1.2841402
- [27] Zhang, Q., He, L., and Rawlinson, A., 2014, "Effects of Inlet Turbulence and End-Wall Boundary Layer on Aerothermal Performance of a Transonic Turbine Blade Tip," *ASME J. Eng. Gas Turbines Power*, **136**(5), pp. 052603. DOI: 10.1115/1.4026002
- [28] Whitehead, D. S., 1987, "Classical Two-Dimensional Methods," Chapter 2 in *AGARD Manual on Aeroelasticity in Axial-Flow Turbomachines*, Issue 1.
- [29] He, L., 1990, "An Euler Solution for Unsteady Flows Around Oscillating Blades," *ASME J. Turbomach.*, **112**(4), pp. 714-722. DOI: 10.1115/1.2927714
- [30] Frey, C., and Kersken, H.-P., 2016, "On the Regularisation of Non-Reflecting Boundary Conditions Near Acoustic Resonance," In *ECCOMAS Congress 2016 VII*

European Congress on Computational Methods in Applied Sciences and Engineering,
Crete Island, Greece. DOI: 10.7712/100016.2344.6536

Figure Captions List

- Fig. 1 Experimental linear cascade configuration for influence coefficient method with only the middle blade (reference '0') oscillating, reproduced from Ref. [7]
- Fig. 2 Contributions of influence coefficients from the blade B0 and its neighbouring blades (IBPA = 0° and k=0.4)
- Fig. 3 Computational mesh around the leading edge and inside the gap over tip surface
- Fig. 4 Axial Mach number contours of a) Transitional turbulent, and b) Fully Turbulent model
- Fig. 5 Steady pressure of different turbulence models
- Fig. 6 Cp distributions for different inlet BL thickness
- Fig. 7 Steady surface pressure distributions at 95% span with different tip clearance gaps
- Fig. 8 Overall aerodynamic damping at k= 0.2 and 0.4
- Fig. 9 Overall aerodynamic damping at 2D mid-span k=0.4 for transitional and fully turbulent models
- Fig. 10 Overall aerodynamic damping at k=0.4 for different tip clearance settings
- Fig. 11 Minimum damping at least stable IBPA
- Fig. 12 Local Damping on Suction Surface at Two Tip Gaps
- Fig. 13 Quasi-steady analysis illustration
- Fig. 14 Evolution of TLV and PV with **uniform inlet** (velocity vectors and vorticity contours on axial cut planes)

- Fig. 15 Evolution of TLV and PV with **profile inlet** (velocity vectors and vorticity contours on axial cut planes)
- Fig. 16 Unsteady pressure responses on the suction surface of blade B0 in subsonic regime for two bending amplitudes
- Fig. 17 Aero-damping variation with IBPA for tuned cascade as predicted by LINSUB (bending mode, $k=0.6$)
- Fig. 18 Overall aerodynamic damping for different configurations at low-speed condition
- Fig. 19 Far- and near-field pressure amplitudes for different ICM and TWM model configurations at low-speed
- Fig. 20 Mach number contour of high-speed case
- Fig. 21 Unsteady pressure responses on the suction surface of the central blade B0 at high-speed condition
- Fig. 22 Overall aerodynamic damping for different configurations at high-speed condition

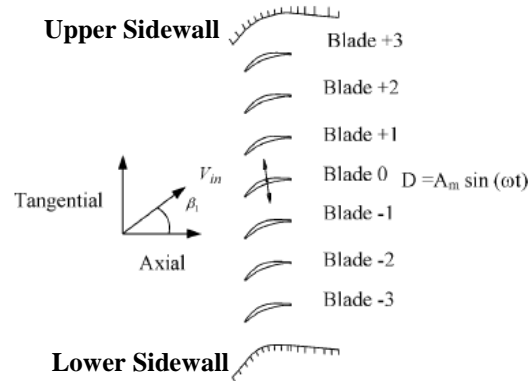


Figure 1: Experimental linear cascade configuration for influence coefficient method with only the middle blade (reference '0') oscillating, reproduced from Ref. [7]

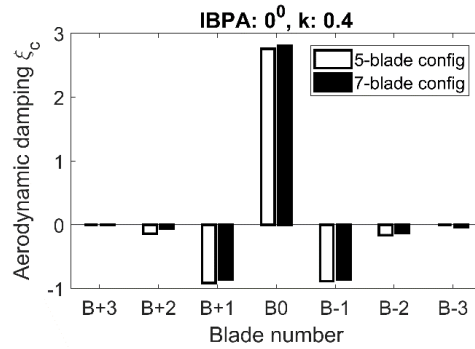


Figure 2: Contributions of influence coefficients from the blade B0 and its neighbouring blades (IBPA = 0° and k=0.4)

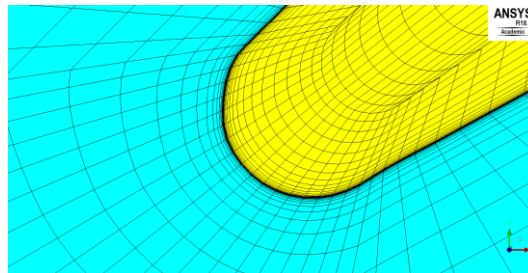


Figure 3: Computational mesh around the leading edge and inside the gap over tip surface

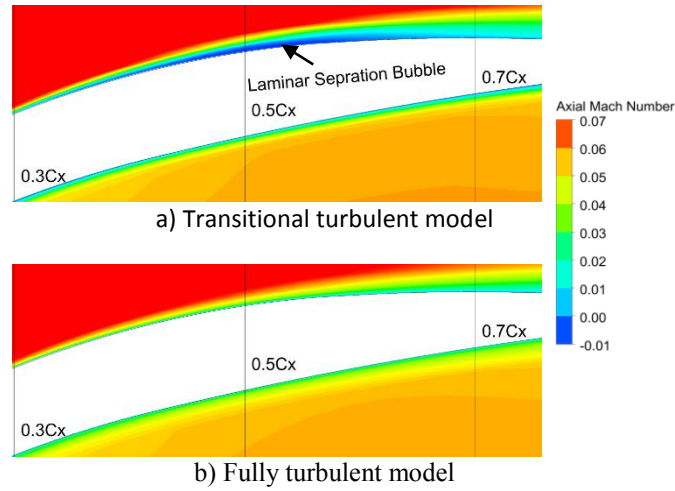


Figure 4: Axial Mach number contours of a) Transitional turbulent, and b) Fully Turbulent model

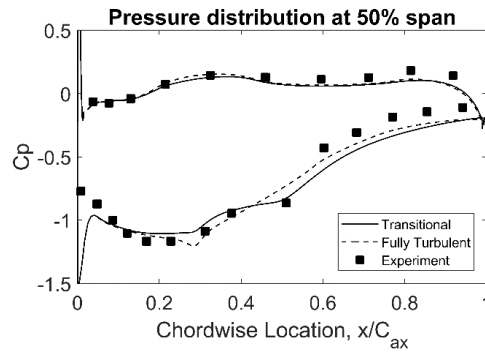


Figure 5: Steady pressure of different turbulence models

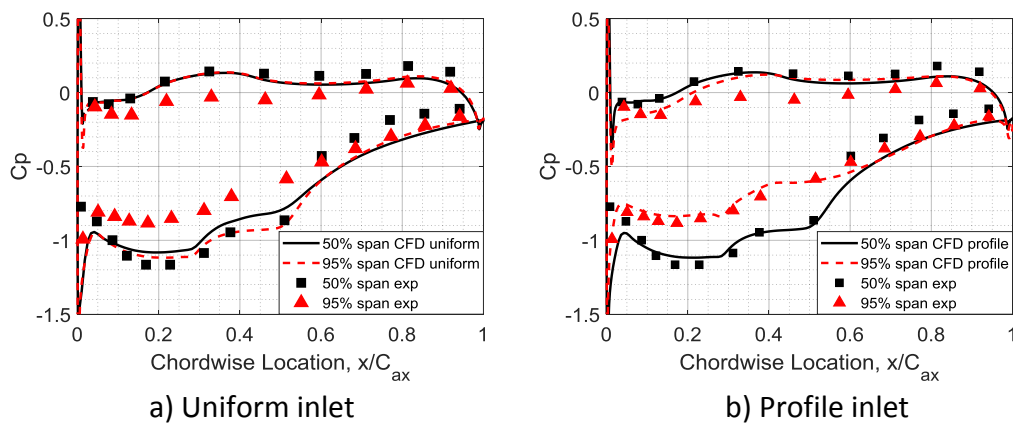


Figure 6: C_p distributions for different inlet BL thickness

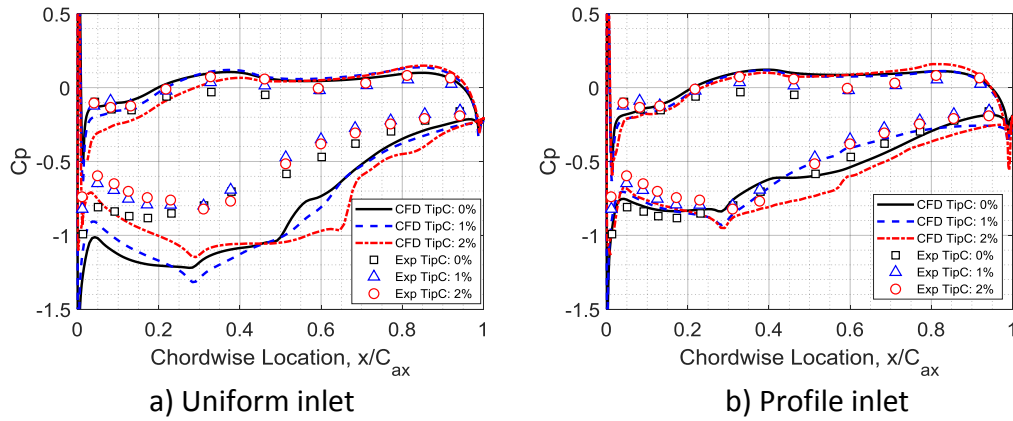


Figure 7: Steady surface pressure distributions at 95% span with different tip clearance gaps

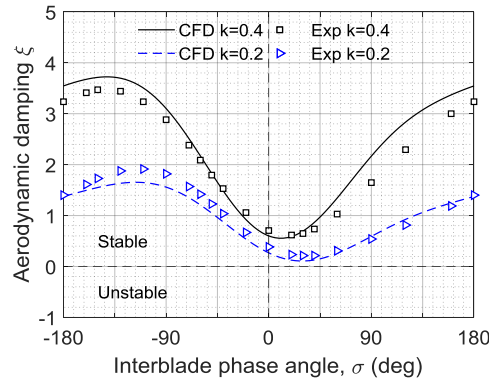


Figure 8: Overall aerodynamic damping at $k = 0.2$ and 0.4

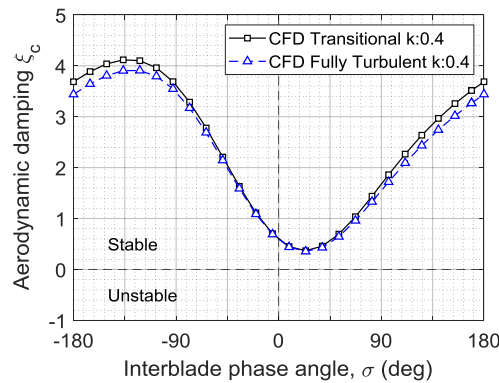


Figure 9: Overall aerodynamic damping at 2D mid-span $k=0.4$ for transitional and fully turbulent models

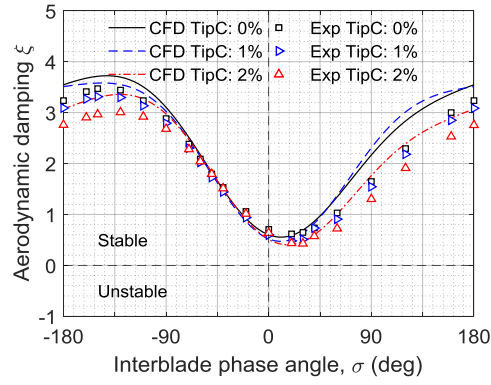


Figure 10: Overall aerodynamic damping at $k=0.4$ for different tip clearance settings

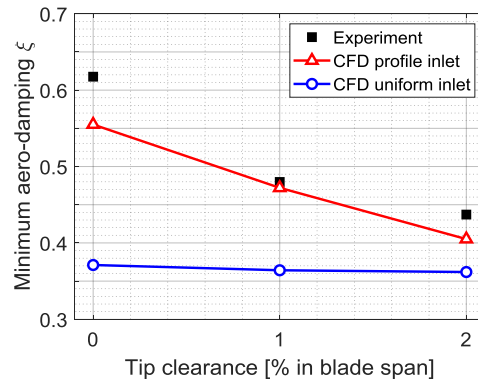


Figure 11: Minimum damping at least stable IBPA

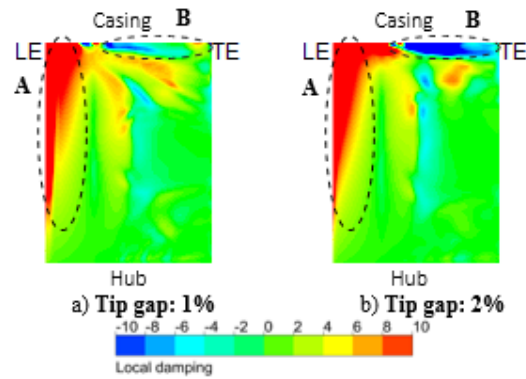
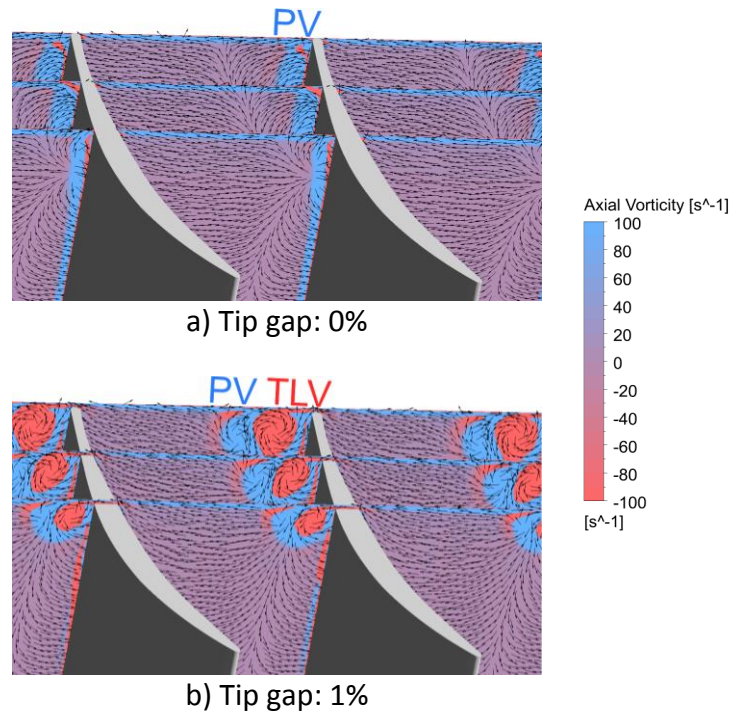
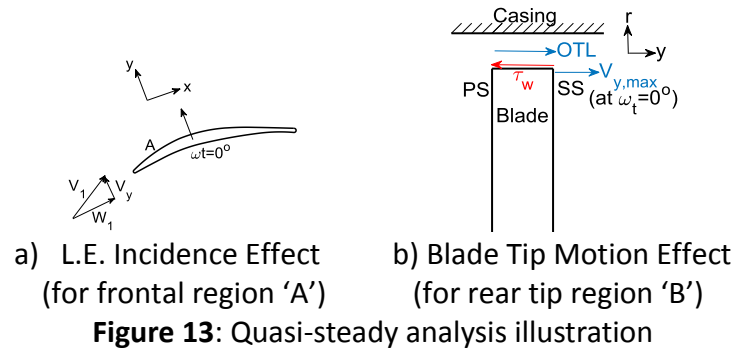


Figure 12: Local Damping on Suction Surface at Two Tip Gaps



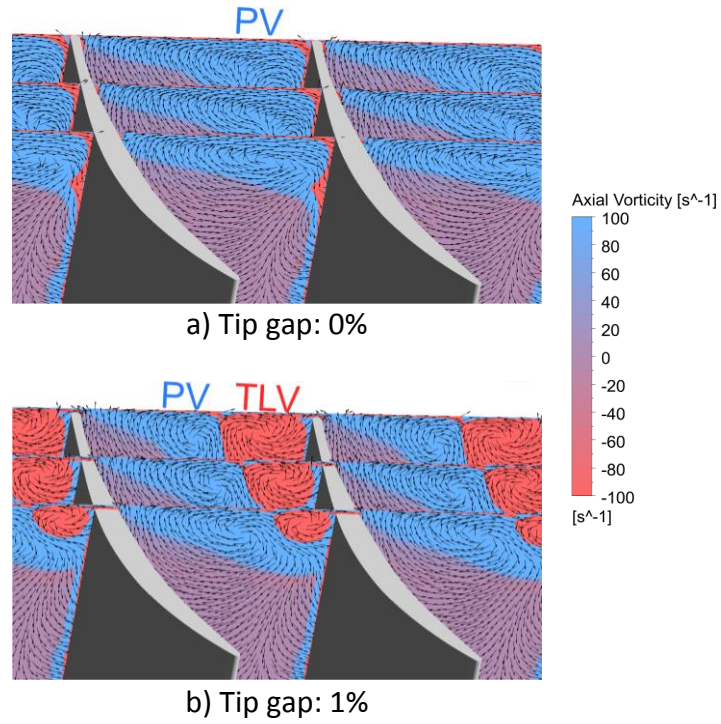


Figure 15: Evolution of TLV and PV with profile inlet (velocity vectors and vorticity contours on axial cut planes)

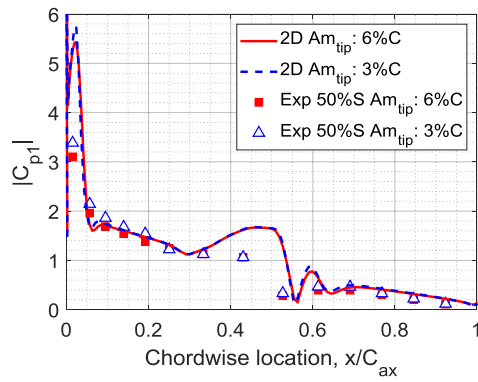


Figure 16: Unsteady pressure responses on the suction surface of blade B0 in subsonic regime for two bending amplitudes

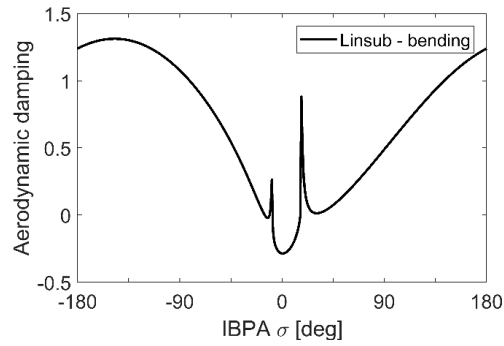


Figure 17: Aero-damping variation with IBPA for tuned cascade as predicted by LINSUB (bending mode, $k=0.6$)

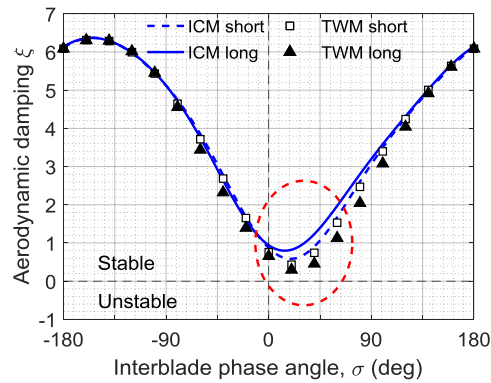


Figure 18: Overall aerodynamic damping for different configurations at low-speed condition

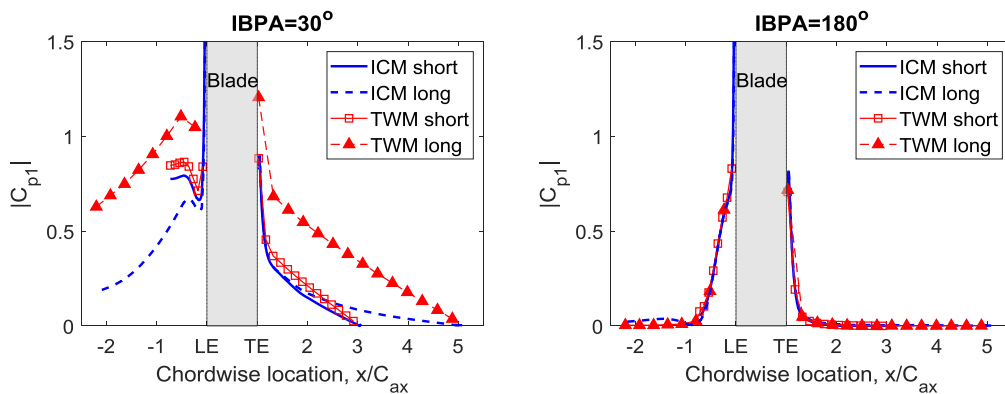


Figure 19: Far- and near-field pressure amplitudes for different ICM and TWM model configurations at low-speed

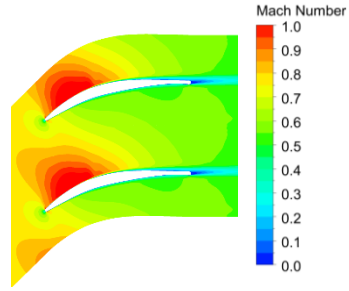


Figure 20: Mach number contour of high-speed case

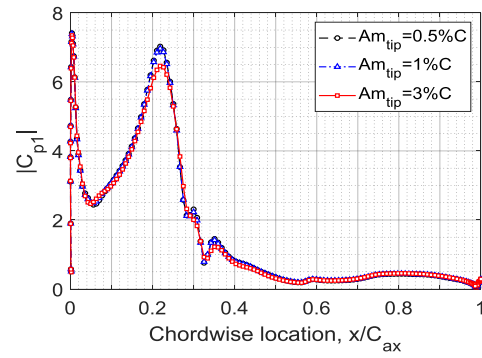


Figure 21: Unsteady pressure responses on the suction surface of the central blade B0 at high-speed condition

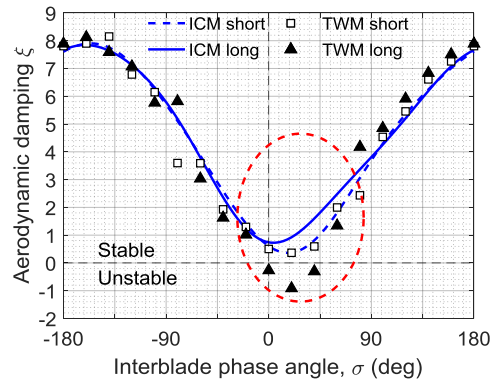


Figure 22: Overall aerodynamic damping for different configurations at high-speed condition

Table Caption List

Table 1	Experimental and Numerical Operating Conditions
---------	---

Table 1 Experimental and Numerical Operating Conditions

Conditions	Experimental	Numerical
Inlet flow angle β_1 , deg	37.5	37.5
Re (based on blade chord and exit velocity)	1.95×10^5	1.967×10^5
Exit isentropic velocity V_{ref} , ms^{-1}	19.5	20.4
Reduced frequency k	0.2, 0.4	0.2, 0.4
Nominal frequency f , Hz	4.14, 8.28	4.33, 8.66
Mode shape	Bending, normal to chord	
Tip bending amplitude Am_{tip}		0.06C
Hub bending amplitude		0.005C